# *Conformational isomerism of trans-[Pt(NH[subscript 2]C[subscript 6]H[subscript 11])[subscript 2]I[subscript 2]] and the classical Wernerian chemistry of [Pt(NH[subscript 2]C[subscript 6]H[subscript 11])[subscript 4]]X[subscript 2] (X=Cl, Br, I)*



**Citation:** Johnstone, Timothy C., and Stephen J. Lippard. "Conformational Isomerism of Trans-[Pt(NH[subscript 2]C[subscript 6]H[subscript 11])[subscript 2]I[subscript 2]] and the Classical Wernerian Chemistry of [Pt(NH[subscript 2]C[subscript 6]H[subscript 11])[subscript 4]]X[subscript 2] (X=Cl, Br, I)." Polyhedron 52 (2013): 565–575.

**As Published:** http://dx.doi.org/10.1016/j.poly.2012.08.010

**Publisher:** Elsevier

**Persistent URL:** http://hdl.handle.net/1721.1/110609

**Version:** Author's final manuscript: final author's manuscript post peer review, without publisher's formatting or copy editing

Published in final edited form as:
*Polyhedron*. 2013 March 1; 52(22): 565–575. doi:10.1016/j.poly.2012.08.010.

# Conformational Isomerism of *trans*-$[Pt(NH_2C_6H_{11})_2I_2]$ and the Classical Wernerian Chemistry of $[Pt(NH_2C_6H_{11})_4]X_2$ (X = Cl, Br, I)[1]

**Timothy C. Johnstone** and **Stephen J. Lippard***
Department of Chemistry, Massachusetts Institute of Technology, Cambridge, MA, 02139

## Abstract

X-ray crystallographic analysis of the compound *trans*-$[Pt(NH_2C_6H_{11})_2I_2]$ revealed the presence of two distinct conformers within one crystal lattice. This compound was studied by variable temperature NMR spectroscopy to investigate the dynamic interconversion between these isomers. The results of this investigation were interpreted using physical (CPK) and computational (molecular mechanics and density functional theory) models. The conversion of the salts $[Pt(NH_2C_6H_{11})_4]X_2$ into *trans*-$[Pt(NH_2C_6H_{11})_2X_2]$ (X = Cl, Br, I) was also studied and is discussed here with an emphasis on parallels to the work of Alfred Werner.

### Keywords

Conformational isomerism; variable temperature NMR; molecular mechanics; density functional theory; coordination chemistry; ionization isomerization; Alfred Werner

## 1. Introduction

### 1.1. The Past

Alfred Werner is rightly termed the “Founder of Coordination Chemistry”[1], for it was by his intellectual power that coordination chemistry, as we know it today, was born. Another title appropriately bestowed on Werner is the “Founder of Inorganic Stereochemistry”. Indeed, it was as a result of “his work on the linkage of atoms in molecules, by which he has thrown fresh light on old problems and opened new fields of research, particularly in inorganic chemistry” that the *Kungliga Vetenskapsakademien* awarded him the Nobel Prize in 1913 [2]. Given the magnitude of his impact on the field of inorganic chemistry, it is easy to overlook the fact that Werner was initially trained as an organic chemist, and his early work on the stereochemistry of nitrogen centers presaged his later foray into inorganic stereochemistry [3, 4]. The spatial arrangement of atoms featured prominently in Werner’s

[1]Dedicated to the memory of Alfred Werner on the 100th anniversary of his Nobel Prize in Chemistry.



*Corresponding author: Tel.: (617) 253-1892, Fax: (617) 258-8150, lippard@mit.edu, Mailing address: 77 Massachusetts Ave., Building 18, Room 498, Cambridge, MA, 02139.

Supplementary data

Tables of selected crystallographically determined bond lengths and angles are presented as Supplementary data along with the Cartesian coordinates of DFT optimized molecular geometries and the details of the calculation described in Section 3.4. CCDC 882679 – 882684 contain the supplementary crystallographic data for compounds **1** – **6**. These data can be obtained free of charge via http://www.ccdc.cam.ac.uk/conts/retrieving.html, or from the Cambridge Crystallographic Data Centre, 12 Union Road, Cambridge CB2 1EZ, UK; fax: (+44) 1223-336-033; or deposit@ccdc.cam.ac.uk.

work, and it was by the preparation of isomeric, particularly stereoisomeric, species that he firmly established his coordination theory [5].

The first report of isomerism, that of isocyanic and fulminic acid, was recorded by Liebig and Wöhler in the 1820's [6] and the term *isomer* was later coined by Berzelius to describe compounds of identical atomic composition but otherwise varying in properties [7]. Many forms of isomerism are now recognized and can be largely divided into two categories: structural isomers, which differ in the chemical linkage of atoms, and stereoisomers, which differ only in the spatial arrangement of similarly bonded atoms [8].

Stereoisomers typically take front stage in discussions of Werner's work, but one form of inorganic stereoisomerism that was not explicitly treated by Werner is *conformational isomerism* [9]. Complex isomers of this type share a common atomic connectivity, (i.e. they are not structural isomers) and ligand distribution about the metal center (i.e. not geometric isomers) but are diastereomeric (i.e. not optical isomers). A manner by which this set of criteria can be satisfied is hindered rotation within a molecule [10]. This isomerism was first recognized in coordination compounds in 1970 during an investigation of two isomeric forms of $[Co(NO_2)_3NH_3(en)]$ [11]. It was uncovered by X-ray crystallographic analysis that the two forms were related by rotation about a single $Co–N_{nitrite}$ bond [12]. Although the significance of the discovery was not fully appreciated, Werner may have isolated these two different forms of the molecule over half a century earlier [13].

Werner also conducted a large body of work on a host of structural isomers [9]. One particular form of isomerism in the Wernerian classification was termed *ionization isomerism,* whereby two species sharing the same elemental composition form different ions upon dissolution. For example, $[Co(NH_3)_4Cl_2]Br$ and $[Co(NH_3)_4ClBr]Cl$ constitute a pair of ionization isomers. Interconversion between these two species is tantamount to exchange of an inner sphere for an outer sphere ligand. Variations on this motif, although not strictly ionization isomerizations, were critical in preparing the material used by Werner and Jørgensen in defense of their respective theories of the geometries of transition metal compounds. For instance, Jørgensen reported that cobalt(III) chloride can be converted from the *luteo* to the *purpureo* form when heated to temperatures greater than 100 °C [14]. In this reaction, a chloride ion from the outer sphere of $[Co(NH_3)_6]Cl_3$ exchanges with an inner sphere ammine ligand to afford $[Co(NH_3)_5Cl]Cl_2$.

### 1.2. The Present

During the course of an investigation of the chemistry of an intermediate in the synthesis of the anticancer agent satraplatin [15], *cis*, *cis*, *trans*-$[Pt(NH_3)(NH_2C_6H_{11})Cl_2(OOCCH_3)_2]$, we obtained the crystal structure of *trans*-$[Pt(NH_2C_6H_{11})_2I_2]$. In a single crystal of this compound, there is a pair of conformational isomers having both syn and anti disposition of the cyclohexylamine rings with respect to the plane containing platinum and its four bonded atoms. We were therefore interested to determine whether the two isomers could be resolved and whether it might be possible to observe dynamic exchange between them. When preparing *trans*-$[Pt(NH_2C_6H_{11})_2I_2]$, we encountered reactivity paralleling that of the aforementioned conversion of *luteo* to *purpureo* cobalt(III) ammine chlorides, whereby the halide salts of the $[Pt(NH_2C_6H_{11})_4]^{2+}$ cation, $[Pt(NH_2C_6H_{11})_4]X_2$, converted to *trans*-$[Pt(NH_2C_6H_{11})_2X_2]$ upon heating (Scheme 1). This chemistry, together with model studies ranging from hand-held CPK representations, to molecular mechanics (MM), to density functional theory (DFT) calculations are reported herein.

## 2. Experimental

### 2.1. General methods and materials

Potassium tetrachloroplatinate(II) was purchased from Strem Chemicals and used as received. Cyclohexylamine was used as received from Sigma Aldrich. Potassium halide salts were obtained from Mallinckrodt and used as received. Reactions were carried out under normal atmospheric conditions, although care was taken to avoid excessive exposure of the platinum complexes to light, particularly when heated in solution.

### 2.2. Physical measurements

NMR spectral measurements were carried out using a Varian Inova 500 spectrometer housed in the MIT Department of Chemistry Instrumentation Facility (DCIF) and spectra were processed using *Mnova Lite*. $^{1}H$ and $^{13}C\{^{1}H\}$ NMR spectra were referenced to residual internal solvent signals and resonances are reported in ppm as chemical shifts (δ) with respect to tetramethylsilane (δ 0 ppm). $^{195}Pt\{^{1}H\}$ NMR spectra were referenced externally to a 0.3 M solution of $K_2PtCl_4$ in $D_2O$ (δ −1628 ppm) and resonances are reported in ppm referenced to $K_2PtCl_6$ in $D_2O$ (δ 0 ppm). FTIR spectra were collected on a ThermoNicolet Avatar 360 spectrophotometer using the *OMNIC* software. Samples were prepared as KBr pellets. Melting points were obtained using a Mel-temp electrothermal melting point apparatus. ESI-MS measurements were performed on an Agilent Technologies 1100 series LC/MSD ion trap. A commercial analytical laboratory performed the elemental analyses.

### 2.3. Synthesis of $[Pt(NH_2C_6H_{11})_4]Cl_2$ (1)

A red solution of potassium tetrachloroplatinate(II) (200 mg, 0.48 mmol) in 4 mL of water was treated with cyclohexylamine (1 mL, 8.7 mmol) and heated to 100 °C in the dark. After 30 min at reflux, the reaction mixture, a suspension of a white solid in a colorless solution, was removed from heat, cooled to room temperature, and then further cooled in an ice bath for 4 h. After this time, the mixture was filtered and the filtrate was collected for crystallization (*vide infra*). The off-white precipitate isolated was washed with cold water, cold ethanol, and diethyl ether to provide a white solid. The solid was dried in a desiccator. Yield: 184 mg, 58%. M.p. 226–227 °C (decomposition to black solid). The reaction product has low solubility in water and common organic solvents but it dissolves in DMF at temperatures above 50 °C, resulting in a chemical transformation of the compound as described in Section 2.5. With gentle heating (not above 50 °C) enough material dissolved to allow for characterization by mass spectrometry. ESI-MS (positive mode): $m/z$ = 100.1 ($[NH_3C_6H_{11}]^+$, Calc. 100.1), 295.8 ($[M]^{2+}$, Calc. 295.7), 392.2 ($[M\text{-}(NH_2C_6H_{11})_2\text{-}H]^+$, Calc. 392.2), 528.4 ($[M\text{-}(NH_2C_6H_{11})\text{+}Cl]^+$, Calc. 528.1), 590.3 ($[M\text{-}H]^+$, Calc. 590.4). IR (KBr pellet, $cm^{-1}$): 3177 s, 3110 s, 3041 m, 2929 s, 2853 s, 1640 m, 1578 m, 1452 m, 1384 m, 1242 m, 1158 m, 1054 m, 956 w, 896 w, 846 w, 806 w, 767 w, 458 w. Anal. Calc. for $C_{24}H_{52}Cl_2N_4Pt$: C 43.50, H 7.91, N 8.45. Found: C 43.25, H 8.31, N 8.34.

### 2.4. Synthesis of trans-$[Pt(NH_2C_6H_{11})_2I_2]$ (6) using $HI_{(aq)}$

To a suspension of compound **1** (80 mg, 0.12 mmol) in 3 mL of water was added 7 M hydriodic acid (2 mL, 14 mmol). No reaction was evident until the mixture was heated to 90 °C. At this temperature, the suspended solid gradually turned yellow. After 6 h, the reaction was removed from the heat, cooled to room temperature, and the yellow precipitate was collected by filtration. The yellow solid was washed with water and then dried. Yield: 71 mg, 92%. M.p. 206–208 °C (decomposition to a black liquid). $^{1}H$ NMR (DMF-$d_7$, 500 MHz): δ 4.24 (s, 2H), 3.01 (s, 1H), 2.29 (s, 2H), 1.69 (s, 2H), 1.54 (d, 6 Hz, 1H), 1.22 (m, 9 Hz, 4H), 1.11 (s, 1H). $^{13}C\{^{1}H\}$ NMR (DMF-$d_7$, 125 MHz): δ 58.34, 35.54, 26.40,

25.83. $^{195}$Pt{$^{1}$H} (DMF-$d_7$, 107 MHz): −3331. IR (KBr pellet, cm$^{-1}$): 3274 m, 3243 m, 3196 m, 3113 w, 2930 vs, 2855 s, 1565 s, 1446 m, 1385 m, 1230 m, 1195 m, 1052 m, 1038 w, 893 w. ESI-MS (negative mode) $m/z$ = −773.9 ([M+I]$^-$, Calc. −773.9). Anal. Calc. for $C_{12}H_{26}I_2N_2Pt$: C 22.27, H 4.05, N 4.33. Found: C 22.45, H 3.69, N 4.18.

### 2.5. Reaction observed upon heating 1

In order to characterize the solid obtained in the above-described synthesis of **1** (Section 2.3), attempts were made to dissolve the solid in a variety of solvents, but no appreciable dissolution occurred. We did observe, however, that when the colorless solid was heated in DMF, the powder was consumed and the solution acquired a yellow color. The solution was analyzed by ESI-MS (positive mode) $m/z$ = 527.5 ([**1**-($NH_2C_6H_{11}$)+Cl]$^+$, Calc. 527.2). After cooling to room temperature, yellow prisms deposited and were analyzed by X-ray crystallography as described in Section 2.11.2.

### 2.6. Synthesis of trans-[Pt($NH_2C_6H_{11}$)$_2$Cl$_2$] (2)

Compound **1** (121 mg, 0.18 mmol) was suspended in DMF (15 mL). The mixture was sonicated to disperse the solid and heated to 120 °C for 3 h. After this time, the reaction mixture was a homogenous yellow solution. The solution was concentrated to dryness and the remaining residue was dissolved in a minimal amount of hot $CH_2Cl_2$. Addition of hot hexanes followed by cooling to −40 °C induced crystallization. The off-white crystalline solid was collected by filtration and washed with hexanes and diethyl ether. Yield: 64 mg, 75%. M.p. 244–245 °C (decomposition to black solid). $^{1}$H NMR (DMF-$d_7$, 500 MHz): δ 4.29 (s, 2H), 2.80 (s, 1H), 2.34 (d, J = 11 Hz, 2H), 1.70 (b, J = 12 Hz, 2H), 1.54 (d, J = 12 Hz, 1H), 1.22 (m, 4H), 1.11 (m, 1H). $^{13}$C{$^{1}$H} NMR (DMF-$d_7$, 125 MHz): δ 55.64, 34.86, 26.51, 25.82. $^{195}$Pt{$^{1}$H} (DMF-$d_7$, 107 MHz): −2214. IR (KBr pellet, cm$^{-1}$): 3231 s, 3204 s, 3135 m, 2929 s, 2855 s, 1582 m, 1450 m, 1247 m, 1202 m, 1162 m, 1057 m, 895 w, 847 w. ESI-MS (negative mode) $m/z$ = −499.1 ([M+Cl]$^-$, Calc. −499.1). Anal. Calc. for $C_{12}H_{26}Cl_2N_2Pt$: C 31.64, H 5.64, N 6.03. Found: C 32.03, H 5.48, N 6.03.

### 2.7. Synthesis of [Pt($NH_2C_6H_{11}$)$_4$]Br$_2$ (3)

Potassium tetrachloroplatinate(II) (200 mg, 0.48 mmol) was dissolved in water (5 mL) and to the resulting red solution was added potassium bromide (2.3 g, 19.27 mmol). After heating to 100 °C for 1 h, the solution became a deep orange color, signifying the formation of the tetrabromoplatinate(II) anion. Cyclohexylamine (1mL, 8.7 mmol) was added to the hot solution and a yellow solid immediately began to precipitate. The mixture was stirred at 100 °C for 1 h, after which time the reaction mixture comprised a white precipitate suspended in a colorless solution. The mixture was removed from heat and cooled to 4 °C overnight. The off-white solid was collected by filtration and washed with cold water and cold ethanol to afford a white solid. Yield: 299 mg, 83%. M.p. 205–207 °C (decomposition to black solid). As with compound **1**, the solid is insoluble, precluding NMR characterization. With gentle heating (not above 50 °C) enough material dissolved to allow for characterization by mass spectrometry without substantial conversion to **4**. ESI-MS (positive mode) $m/z$ = 100.1 ([$NH_3C_6H_{11}$]$^+$, Calc. 100.1), 295.7 ([M]$^{2+}$, Calc. 295.7), 392.2 ([M-($NH_2C_6H_{11}$)$_2$-H]$^+$, Calc. 392.2), 572.3 ([M-($NH_2C_6H_{11}$)+Br]$^+$, Calc. 572.2). IR (KBr pellet, cm$^{-1}$): 3194 s, 3110 s, 3037 s, 2939 s, 2849 s, 1600 m, 1544 m, 1455 m, 1263 m, 1169 m, 1059 m, 1045 m, 895 m, 452 w. Anal. Calc. for $C_{24}H_{52}Br_2N_4Pt$: C 38.35, H 6.97, N 7.45. Found: C 38.48, H 6.85, N 7.33.

### 2.8. Synthesis of trans-[Pt($NH_2C_6H_{11}$)$_2$Br$_2$] (4)

The reaction was carried out as described above for the synthesis of **2** except that 290 mg (0.39 mmol) of **3** were used. The product was isolated as a pale yellow crystalline solid.

Yield: 114 mg, 54%. M.p. 224–225 °C (decomposition to black liquid). $^{1}$H NMR (DMF-$d_7$, 500 MHz): δ 4.26 (s, 2H), 2.88 (s, 1H), 2.33 (d, J = 9.5 Hz, 2H), 1.69 (d, J = 11 Hz, 2H), 1.54 (d, 13.5 Hz, 1H), 1.26 (m, 4H), 1.10 (s, 1H). $^{13}$C{$^{1}$H} NMR (DMF-$d_7$, 125 MHz): δ 56.55, 35.14, 26.49, 25.80. $^{195}$Pt{$^{1}$H} (DMF-$d_7$, 107 MHz): −2584. IR (KBr pellet, cm$^{-1}$): 3228 s, 3203 s, 3130 m, 2927 s, 2856 s, 1576 m, 1449 m, 1393 m, 1340 m, 1243 m, 1201 m, 1160 m, 1057 m, 1045 m, 963 w, 893 m, 846 w, 793 w, 737 w. ESI-MS (negative mode) $m/z$ = −633.0 ([M+Br] $^{-}$, Calc. −632.9). Anal. Calc. for $C_{12}H_{26}Br_2N_2Pt$: C 26.05, H 4.74, N 5.06. Found: C 26.45, H 4.46, N 4.94.

### 2.9. Synthesis of [Pt(NH$_2$C$_6$H$_{11}$)$_4$]I$_2$ (5)

The reaction was carried out on the same scale as described above for the synthesis of **3**, using potassium iodide (3.2 g, 19.27 mmol) instead of potassium bromide. The product was isolated as a colorless solid. Yield: 384 mg, 94%. M.p. 177–180 °C (decomposition to orange liquid, slight yellowing of the solid observed beginning at 167 °C). Unlike **1** and **3**, **5** is readily soluble in DMF at room temperature. $^{1}$H NMR (DMF-$d_7$, 500 MHz): δ 5.24 (s, 8H), 2.81 (s, 4H), 2.47 (d, J = 11 Hz, 8H), 1.74 (d, J = 14 Hz, 8H), 1.60 (d, 13 Hz, 4H), 1.47 (q, J = 12 Hz, 8H), 1.32 (q, 13 Hz, 8H), 1.09 (q, 13 Hz, 4H). $^{13}$C{$^{1}$H} NMR (DMF-$d_7$, 125 MHz): δ 56.69, 34.80, 26.26, 26.02. IR (KBr pellet, cm$^{-1}$): 3192 s, 3108 s, 3038 s, 2933 s, 2853 s, 1596 m, 1564 m, 1450 m, 1264 m, 1165 m, 1059 m, 1045 m, 895 m, 752 m, 458 w. ESI-MS (positive mode) $m/z$ = 295.7 ([M]$^{2+}$, Calc. 295.7), 392.2 ([M-(NH$_2$C$_6$H$_{11}$)$_2$-H]$^{+}$, Calc. 392.2), 590.4 ([M-H]$^{+}$, Calc. 590.4), 619.2 ([M-(NH$_2$C$_6$H$_{11}$)+I]$^{+}$, Calc. 619.2). Anal. Calc. for $C_{24}H_{52}I_2N_4Pt$: C 34.09, H 6.20, N 6.63. Found: C 34.23, H 5.54, N 6.49.

### 2.10. Synthesis of trans-[Pt(NH$_2$C$_6$H$_{11}$)$_2$I$_2$] (6)

The reaction was carried out as described above for the syntheses of **2** and **4** except that 359 mg (0.42 mmol) of **5** were used. The product was isolated as a yellow crystalline solid. Yield: 151 mg, 55%. M.p. 206–208 °C (decomposition to black liquid). The characterization is identical to that reported in Section 2.4 for the synthesis of **6** via reaction of **1** with HI$_{(aq)}$.

### 2.11. X-ray crystallography

Single crystals were grown as described below, mounted on a nylon cryoloop in Paratone oil, and cooled to 100 K under a stream of nitrogen. A Bruker APEX CCD X-ray diffractometer controlled by the *APEX2* software [16] was used to collect the diffraction of graphite-monochromated Mo Kα radiation (λ = 0.71073 Å) from the crystal. The data were integrated with *SAINT* [17] and absorption, Lorentz, and polarization corrections were calculated by *SADABS* [18]. Space group determination was carried out by analyzing the metric symmetry and systematic absences of the diffraction pattern with *XPREP* [19]. Using the *SHELXTL-97* software package [20, 21], structures were solved by either Patterson or direct methods and refined against $F^2$. Refinement was carried out using standard procedures [22]. All, including hydrogen, atoms were located in the difference Fourier map during refinement. Hydrogen atoms were placed at calculated positions and refined with their isotropic displacement parameters ($U_{iso}$) set equal to 1.5, for terminal $CH_3$ groups, or 1.2, for secondary and tertiary carbons and nitrogens, times the $U_{iso}$ of the atom to which they are attached. Specific refinement details are reported below and CIF data are provided for all structures in the Supplementary data along with tables of bond lengths and angles. All structures have been deposited in the Cambridge Structural Database. Pertinent crystallographic parameters are collected in Table 1. All structures were checked for missed higher symmetry and twinning with *PLATON* [23] and were further validated using *CheckCIF*.

**2.11.1. Structural analysis of $[Pt(NH_2C_6H_{11})_4]Cl_2$ (1)—**Vapor diffusion of ethanol into the aqueous filtrate of the reaction mixture that yielded **1** afforded colorless blocks. The asymmetric unit contained a chloride ion and half of the complex cation of **1.** The platinum sits on an inversion center, the action of which generates the full molecule. No solvent co-crystallizes with the complex and the chloride counterions act as hydrogen bond acceptors for the amine donors. No disorder was present in the structure and the largest residual electron density peak (0.85 e $Å^{-3}$) and hole (−0.68 e $Å^{-3}$) were located 0.80 Å and 0.76 Å from the platinum atom, respectively.

**2.11.2. Structural analysis of trans-$[Pt(NH_2C_6H_{11})_2Cl_2]$•2DMF (2•2DMF)—**As described in Section 2.5, when **1** is suspended in DMF and heated, the solid dissolves and produces a yellow solution. When this solution is allowed to stand at room temperature overnight, yellow prisms formed. The prisms formed in this manner appear to be highly twinned judging from the appearance of split spots in the diffraction pattern. A fragment was broken off of a prismatic crystal and appeared to contain a single domain. Although the metric parameters of the crystal approximate those of a monoclinic system, a satisfactory refinement could only be obtained in space group P $\bar{1}$. The asymmetric unit of the crystal contained half of a molecule of **2** and a molecule of DMF. The platinum atom sits on an inversion center and application of this symmetry operation generates the full molecule in the anti conformation. This structure is the DMF solvate of a structure previously reported in the literature [24]. No disorder was present in the structure and the largest residual electron density peak (1.01 e $Å^{-3}$) and hole (−0.73 e $Å^{-3}$) were located 0.87 Å and 0.79 Å from the platinum atom, respectively.

**2.11.3. Structural analysis of $[Pt(NH_2C_6H_{11})_4]Br_2$ (3)—**Colorless prisms of **3** were grown by slow evaporation of a DMF solution. To obtain an untwinneduntwinned sample, we broke off a fragment from a larger crystal. The asymmetric unit contains one half of the cation of **3** and a bromide counterion. The platinum complex sits on an inversion center generating the full molecule. No solvent was present in the lattice and there was no evidence of twinning or disorder. The largest residual electron density peak (1.97 e $Å^{-3}$) and hole (−0.82 e $Å^{-3}$) were located 0.83 Å and 0.55 Å from the platinum and bromine atoms, respectively.

**2.11.4. Structural analysis of trans-$[Pt(NH_2C_6H_{11})_2Br_2]$ (4)—**Large yellow prisms were obtained by slow evaporation of an acetone solution of **4**. A fragment was broken off from a larger crystal and mounted on the diffractometer. The asymmetric unit of the crystal contained half of a molecule of **4** with the platinum atom sitting on an inversion center. The full molecule is therefore present in the anti conformation. This structure is isomorphous with one previously reported in the literature [25]. In this previous study, the collection was carried out at room temperature and the hydrogen atoms were not included in the model. No disorder was present in the structure reported here and the largest residual electron density peak (1.01 e $Å^{-3}$) and hole (−1.25 e $Å^{-3}$) were located 0.74 Å and 0.77 Å from the platinum atom, respectively.

**2.11.5. Structural analysis of $[Pt(NH_2C_6H_{11})_4]I_2$ (5)—**Colorless needles of **5** were grown by slow evaporation of a DMF solution. The asymmetric unit comprises one half of the cation of **5** and an iodide counterion. The platinum complex sits on an inversion center generating the full molecule. No solvent was present in the lattice and there was no evidence of twinning or disorder. The largest residual electron density peak (1.02 e $Å^{-3}$) and hole (−0.71 e $Å^{-3}$) were located 0.81 Å and 0.84 Å from the platinum and bromine atoms, respectively.

**2.11.6. Structural analysis of trans-[Pt($NH_2C_6H_{11}$)$_2$$I_2$] (6)—**Yellow needles were consistently obtained when attempting to grow crystals of the iodo-bridged complex [Pt($NH_2C_6H_{11}$)I(μ-I)]$_2$. This compound was prepared as described previously [26]. A crystal was selected from a crop of needles grown by slow evaporation of a DMF solution of [Pt($NH_2C_6H_{11}$)I(μ-I)]$_2$. The asymmetric unit contained 1.5 molecules of **6**. The full molecule in the asymmetric unit is present in the syn conformation and the inversion center generates the anti conformation from the half-molecule that sits on this special position. No solvent molecules were present in the structure and no disorder was detected. The largest residual electron density peak (1.29 e Å$^{-3}$) and hole (−0.80 e Å$^{-3}$) were located 0.86 Å and 0.66 Å from Pt2 and I12, respectively (a complete atom-labeling scheme is depicted in Figure 1).

## 2.12. Variable temperature (VT) NMR

To interrogate the potential dynamic conversion between the syn and anti conformers of **6**, the NMR spectrum of this compound was acquired at low temperature. In DMF-$d_7$, the solution could be cooled to −55 °C, before reaching the solvent freezing point. At this temperature, no de-coalescence was observed. Dichlorofluoromethane (DCFM, prepared as described in [27]), a solvent that can be super-cooled to −150 °C, was used to access lower temperatures. Solutions of **6** in DCFM-*d* were cooled to −113 °C, but still no de-coalescence was observed. There was, however, a systematic change in the chemical shift of the signal arising from the amine protons over the range 0 °C to −113 °C, which allowed for the determination of the thermodynamic parameters describing the isomerization. The NMR spectrum in DMF-$d_7$ was also recorded at temperatures as high as 60 °C with no significant observed change in the lineshapes of the resonances. At each temperature, the sample was allowed to equilibrate for an additional 2 minutes following a stable thermostat reading, re-locked, shimmed, and then analyzed.

## 2.13. CPK models

Physical models of compounds **2**, **4**, and **6** were constructed using standard CPK plastic models in which the radius of the plastic sphere is proportional to the van der Waals radius of a given atom [28, 29]. A generic “metal” sphere was used for the central platinum atom.

## 2.14. Molecular mechanics (MM) calculations

MM calculations were performed on *Gaussian 03* [30] using the universal force field (UFF) and the corresponding UFF parameters for all atoms [31]. The atomic coordinates of **6** in the anti conformation, as determined by X-ray crystallography, were used as the input geometry following normalization of the C–H and N–H bond lengths to 1.089 Å and 1.015 Å, respectively. This process was carried out with the program *Mercury* to account for the well-established fact that X-ray diffraction analysis underestimates the length of bonds involving hydrogen atoms. A rigid surface scan was carried out along the linear combination of internal coordinates corresponding to rotation of one of the cyclohexylamine ligands about the Pt–N bond. This scan was accomplished by simultaneously incrementing all the I–Pt–N–X dihedral angles, where X represents each atom of one of the cyclohexylamine ligands. That is, at each step of the rigid surface scan, all I–Pt–N–X dihedral angles were increased by a fixed amount (2°) and at each of these geometries a single point energy calculation was carried out. The maximum along this scan was used as an initial guess at the transition state in subsequent DFT calculations. The coordinates of this maximum are tabulated in the Supplementary data. As a practical note, we mention here that due to the initialization procedure of *Gaussian 03*, despite the fact that MM calculations do not employ basis sets, basis sets need to be defined for all atoms in the calculation. The default basis set that is used by *Gaussian 03*, should no basis set be indicated in the input file, is undefined for Pt

and causes the calculation to fail. We have circumvented this difficulty by placing a dummy atom, for which the default basis set is defined, at the position of the platinum and parameterizing it with the UFF parameters for platinum. We have verified that the element chosen for the dummy atom does not affect the outcome of the calculations as long as it is correctly parameterized as a Pt. We chose to use Pd so that the graphics generated have a coloring scheme similar to that expected for Pt.

### 2.15. Density functional theory (DFT) calculations

DFT calculations were also carried out using *Gaussian 03*. The geometries of the syn and anti conformations of **6** were optimized in the gas phase using the hybrid functional PBE0 [32], Ahlrichs' TZVP basis set for C, H, and N, and the LANL2DZ effective core potentials for I and Pt [33, 34]. The atomic coordinates of the respective conformers from the X-ray structure of **6** were used as input for the geometry optimizations. Frequency calculations were performed to confirm that the converged structures were local minima on the potential energy surface (PES) and to provide zero-point energy (ZPE) corrections. A transition state search was performed using the quadratic synchronous transit-guided quasi-Newton (STQN) method, which uses as input the coordinates of the initial and final states of the isomerization and an initial guess for the transition state [35, 36]. The optimized geometries of the anti and syn conformations were used as the start and end structures, respectively, and the coordinates from the maximum of the MM rigid surface scan were used as the initial guess for the transition state. The search converged on a transition state that appeared reasonable in that it corresponded qualitatively with that predicted by the physical CPK models and the MM calculations. A frequency calculation was carried out to confirm that the structure corresponds to a first order saddle point on the PES and to provide a ZPE correction to the total energy. Results were visualized with *GaussView*. The coordinates of the DFT optimized structures of the anti and syn conformations as well as the transition state are tabulated in the Supplementary data.

## 3. Results and Discussion

### 3.1. Crystallization of 6

One route to the platinum(IV) prodrug satraplatin involves the preparation of an iodo-bridged platinum(II) dimer, $[Pt(NH_2C_6H_{11})I(\mu\text{-}I)]_2$. Cleavage of the iodo bridges affords the mixed *cis*-(cyclohexylamine)(ammine)platinum(II) core present in satraplatin [37]. While attempting to crystallographically determine the structure of the iodo-bridged dimer, yellow needles were obtained from a DMF solution. X-ray diffraction analysis revealed these crystals to be composed of *trans*-$[Pt(NH_2C_6H_{11})_2I_2]$ (**6**). As described in Section 2.11.6 and depicted in Figure 1, within the crystal lattice, **6** is present in both syn and anti conformations. The presence of both conformers in the solid state structure might indicate that a high barrier to rotation is present, resulting in stable isomeric species that simply happen to co-crystallize. Alternatively, a lower barrier could be present, with the crystallization process trapping out the two dynamically interconverting isomers.

### 3.2. Preparation of 6

The possibility that compound **6** might exist as two stable conformers prompted the independent synthesis of this molecule. Simple diam(m)nedihaloplatinum(II) species such as **6** are among the oldest known coordination compounds, and the existence of both cis and trans geometric isomers was used by Werner as evidence to support his coordination theory [38]. The classical preparation of the trans isomer, initially known as Jørgensen's reaction, involves treatment of the tetraam(m)ineplatinum(II) cation with hydrohalic acid or heating the halide salt of the cation [39]. This reactivity was initially viewed as standing in contrast to Peyrone's reaction, in which the cis isomer can be prepared by treatment of the

tetrahaloplatinate(II) anion with ammonia/amine [40]. It was not until the work of Chernyaev on the trans effect that these two reactions were understood to be different manifestations of the same basic principle [41, 42]. Compound **6** was prepared by treatment of **1**, itself readily prepared by refluxing $K_2PtCl_4$ with cyclohexylamine [43], with aqueous hydriodic acid (Scheme 2). The desired product can be obtained but the reaction proceeds sluggishly. Moreover, the endpoint is difficult to ascertain because, at the start of the reaction, the material is a white suspension and at the end of the reaction the product is a suspension of yellow solid. Furthermore, compound **1** does not readily dissolve in aqueous solutions, most likely due to the hydrophobic cyclohexylamine ligands, which hampers smooth progression of the reaction.

### 3.3. VT NMR spectral study of 6

Multinuclear ($^1$H, $^{13}$C, and $^{195}$Pt) NMR spectroscopic characterization of the reaction product showed no evidence for the presence of two distinct conformers of **6**, a result consistent with earlier characterization data for this compound [43]. The possibility remained, however, that the two conformers might be dynamically interconverting in solution. Variable temperature NMR studies were carried out to investigate this possibility but no de-coalescence was observed in the $^1$H, $^{13}$C, or $^{195}$Pt NMR spectra recorded at temperatures (−55 °C) just above the freezing point of DMF, nor when a DCFM-*d* solution of **6** was cooled to −113 °C.

Over the course of cooling the solution, a systematic trend in the chemical shift of the amine protons was observed, however, as depicted in Figure 2.

A plot of the chemical shift of the amine peak versus temperature reveals a sigmoidal relationship (Figure 3). This behavior reflects the change in equilibrium distribution of the syn and anti species with changing temperature. The exchange is occurring on the sub-millisecond time scale as evidenced by the single, averaged signal that results. This signal represents the weighted average of signals arising from the two isomers. The observed chemical shift is related to the ratio of the two isomers by eq 1:

$$\delta = \frac{K_{eq}\delta_{anti} + \delta_{syn}}{1 + K_{eq}} \quad (1)$$

By substituting the known dependence of the equilibrium constant on the standard free energy of reaction and the dependence of this parameter in turn on the standard enthalpy and entropy of reaction, we arrive at eq 2. This expression assumes that there is no temperature dependence of the chemical shifts of the NH resonances for both presumed conformers.

$$\delta = \frac{\exp\left(\frac{T\Delta S^\circ - \Delta H^\circ}{RT}\right)\delta_{anti} + \delta_{syn}}{1 + \exp\left(\frac{T\Delta S^\circ - \Delta H^\circ}{RT}\right)} \quad (2)$$

A least-squares fit of this equation to the data (Figure 3) provides values of $\delta_{anti}$ = 3.605 ppm, $\delta_{syn}$ = 3.330 ppm, $\Delta H^\circ$ = 30.127 kJ mol$^{-1}$, and $\Delta S^\circ$ = 139.6 J mol$^{-1}$ K$^{-1}$. The assignment of the anti conformer to the limiting signal at 3.605 ppm and the syn conformer to the signal at 3.330 ppm is based on the computational data – and chemical intuition – that suggest the anti conformation to be slightly lower in energy than the syn. These parameters can be used to calculate the standard Gibbs free energy of isomerization, $\Delta G^\circ_{298.15}$ = −11.5 kJ mol$^{-1}$. As described in Section 3.4, DFT calculations provide an estimate of $\Delta G^\circ_{298.15}$ =

−2.01 kJ $mol^{-1}$. Although the calculated value is only 18 % of the experimentally determined one, the absolute difference between the two is <10 kJ $mol^{-1}$.

To rule out the possibility that the shift in the amine proton resonance arises from some sort of aggregation phenomenon, the VT NMR study was conducted at a series of different concentrations. Over the range of 3.3 to 10 mM, no deviation in the chemical shifts of the signals was observed. Representative spectra at different concentrations and temperatures are reported in the Supplementary data. The lack concentration dependence indicates that the process being observed is most likely not an aggregation phenomenon. Although the computational results presented here support the assignment of the signal shift as arising from changes in the syn-anti equilibrium, we cannot definitively rule out the possibility that some other process might be causing the observed NMR phenomenon.

The failure of the two resonances to separate, even at temperatures as low −113 °C, highlights the low barrier to interconversion between these two species. The height of this barrier was estimated in modeling studies described in the next section.

### 3.4. Modeling

**3.4.1. Physical models—**In order to probe the magnitude of the barrier to rotation and to corroborate the thermodynamic parameters determined above, modeling was carried out at various levels. The first step taken was to build a physical model of the compound. Although rudimentary and highly simplified, this construction process provides a very real and tactile sense of the relative dimensions within the molecule that is not as readily conveyed in computer simulations. Indeed, there is no substitute to “running one’s hands over a molecular model and experiencing the visual-tactile link that it so important for establishing three-dimensionality in our minds. [44]” In Figure 4 is shown a photo of the CPK model of **2**. This chloride-containing complex was chosen for illustration because the smaller halide ligand shows the steric hindrance in a manner that is more readily photographed. Models were built with bromide and iodide ligands as well and similar qualitative conclusions can be drawn. Manual rotation about the Pt–N bond results in a steric clash between a ring C–H group and the halide ligand, as highlighted in the middle of Figure 4. Starting from the anti conformation, manual forcing across this barrier provides access to the syn conformation.

**3.4.2. Molecular mechanics—**Given that the bond between the Pt and the N is a simple σ-type dative coordinate bond, a significant electronic barrier to rotation is not expected. Moreover, the CPK models suggested that direct steric interactions between the cyclohexyl ring and the halide ligand provide the kinetic barrier to isomerization. These facts suggest that a purely mechanical model of the rotation may provide meaningful insight into the process. Molecular mechanics (MM) calculations can provide such information. In fact, one of the first uses of MM was to study the hindered internal rotation of biphenyls [45, 46]. MM calculations are also computationally inexpensive, allowing for relatively large number of geometries to be probed at low cost. The universal force field (UFF) was employed because it has been parameterized for all elements of the periodic table. Although more exact results could be obtained by explicitly parameterizing the force field for the molecule under investigation, the goal of the MM calculations here is only to provide a qualitative description of the rotation process and to gain insight into a potential transition state for the isomerization. Higher level calculations have been used to provide an estimate into the magnitude of the rotational barrier.

The results of a rigid surface scan are presented in Figure 5. As the cyclohexylamine group is rotated about the Pt–N bond, the energy rises. In contrast to ab initio calculations, which calculate energies with respect to the energies of the constituent nuclei and electrons at infinite separation, the energies calculated in MM are reported with respect to a

hypothetically unstrained molecule. The geometry of the maximum along this PES scan occurs, much as one might expect, when the ligand is halfway through the rotation. Specifically, we can see that a cyclohexyl hydrogen, highlighted with a red circle in Figure 5, has been brought in close proximity to a halide ligand, as was seen with the CPK models.

**3.4.3. DFT studies—**DFT calculations were carried out to more accurately estimate the energies of the isomers and the magnitude of the barrier to their interconversion. The geometries of syn and anti conformers were optimized in the gas phase and found to agree well with those from the crystal structure. The absence of vibrations with imaginary frequencies indicates that there are no negative elements in the respective Hessians of the two structures and confirms that they are mimina on their respective PESs. The ZPE corrected difference in free energy between the anti and syn conformers was found to be −2.01 kJ $mol^{-1}$, with the anti being more stable. As described in Section 3.3, this result supports the assignment of the different conformers to their respective chemical shifts.

Given the size and flexibility of the molecule under investigation, it is possible that errors in the computed thermochemical parameters may arise from incorrect partitioning of internal rotations as vibrations in the gas phase statistical mechanical calculations [47]. Indeed, the output from the *Gaussian 03* calculations contains a warning indicating that some of the low energy vibrations modeled as harmonic oscillations may instead correspond to internal rotations. Although it can be difficult to correct the partition functions without a suitable expression for the variation in energy along the coordinate of the internal rotation [48], if a calculated vibrational mode were indeed a hindered internal rotation, then there exists a relationship (eq 3) between the height of the rotational barrier and the harmonic oscillator frequency ($\nu$), the periodicity of the rotation ($\sigma$), and the reduced rotational moment of inertia ($I_r$) [49].

$$V_0 = \frac{8\pi^2 \nu^2 I_r}{\sigma^2} \quad (3)$$

The lowest energy vibrations calculated for both the syn and anti conformations correspond to rotation about the Pt N bond. The barrier to that internal rotation is therefore the barrier to the rotation in which we are interested. The details of the determination of $I_r$, $\nu$, and the barrier height are presented in the Supplementary data. The rotational barrier estimated in this manner is 24.0 kJ $mol^{-1}$, a value that compares favorably with one determined as the difference between the ZPE corrected energies of the ground and transition states, fdetermined below (25.6 kJ $mol^{-1}$). This correspondence indicates that, although internal rotations may have been incorrectly partitioned as harmonic oscillator vibrations, the error introduced appears to be small.

A transition state search was carried out and the optimized geometry of the transition state corresponds to an intuitively reasonable structure with one cyclohexyl ring positioned over a halide ligand. The frequency calculation revealed that there is only one vibration with an imaginary frequency, confirming that the structure is located on a first order saddle point on the PES. Importantly, this vibration corresponds to an internal rotation about the Pt–N bond, which is in agreement with the expectation that the reaction coordinate that passes through the transition state should be the rotation of the cyclohexylamine ligand. The difference in ZPE corrected Gibbs free energies of the anti conformer and the transition state was found to be 25.6 kJ $mol^{-1}$. The difference in energy between these species is depicted in Figure 6, along with a molecular diagram of the transition state. The arrows in the diagram of the transition state represent the vibrational motion of the individual atoms along the vibrational mode calculated to have an imaginary frequency. In Figure 6, it can be appreciated that the

general form of this vibration is an internal rotation of one of the cyclohexylamine ligands about the Pt–N bond. That is, the vibrational vectors lay tangent to circles described by the rotation of the ligand. The calculated rotational barrier approaches the limit of processes that can be detected using dynamic NMR spectroscopy. Using the chemical shifts determined in Section 3.3 as those of the isomers, a rough calculation [50], the details of which are provided in the Supplementary data, reveals that de-coalescence is only expected to occur at temperatures below −150 °C. This result explains why no splitting of the resonances was observed in the VT NMR experiments.

### 3.5. Further reactivity of 1

In the process of characterizing compound **1**, it was observed that heating the colorless solid in DMF caused it to dissolve, affording a bright yellow solution. The color change indicated the occurrence of a reaction, and mass spectrometric analysis of the solution showed it to contain the $[Pt(NH_2C_6H_{11})_3Cl]^+$ cation. Moreover, when the solution was allowed to stand at room temperature overnight, yellow prisms formed. Single crystal X-ray diffraction analysis of these prisms showed them to contain compound **2**. This small-scale experiment indicated that, on heating, the outer sphere chloride ligands exchange with the inner sphere cyclohexylamine ligands. This reactivity parallels some of the earliest reactions carried out by Werner and Jørgensen as they developed systematic series of compounds in support of their respective theories on the structures of transition metal complexes [5].

We verified that the conversion of **1** to **2** in this manner can occur on a bulk scale as had previously been reported for the conversion of **5** to **6** under different reaction conditions [43, 51]. Moreover, we found that the method here is generalizable to the bromo and iodo salts of $[Pt(NH_2C_6H_{11})_4]^{2+}$, compounds **3** and **5,** respectively, affording compounds **4** and **6**. Complexes **2**, **4**, and **6** are readily purified by recrystallization from hot $CH_2Cl_2$/hexanes. The compounds become increasing soluble in $CH_2Cl_2$ as we proceed from **2** to **6**, undoubtedly due to the increase in polarizability of the halide ligand.

### 3.6. Characterization of 2, 4, and 6

These three compounds display spectroscopic properties consistent with their formulations as well as the trends expected by systematic alteration of the halide. For instance, the $^{195}Pt$ NMR chemical shifts of compounds **2**, **4**, and **6** are −2214, −2584, and −3331 ppm, respectively. This progression is consistent with the greater degree of covalent character expected in the Pt X bond as we move down the halogens, owing to the decrease in halide hardness, particularly in light of the soft [52], or class b [53], character of Pt(II). This trend also parallels that expected from the variation in electronegativity as we move up the halogen family. As the elements become more electronegative, they donate less electron density to the metal center and shift the $^{195}Pt$ NMR signal downfield. The lack of a significant effect of the halogen on the $^1H$ NMR chemical shifts of the amine protons is consistent with the trans geometry of these compounds. The IR data are consistent with the presence of amine groups and aliphatic C–C and C–H groups [43], but the diagnostic bands arising from Pt X (X = halide) vibrations occur at energies lower than we could probe experimentally in this study.

Crystal structures were previously reported for compounds **2** and **4** [24, 25]. We collected a new data set for an identical polymorph of **4** at low temperature and obtained a higher resolution structure. The structure of **2** reported here is a solvate [54] of the previously reported structure and again the newly collected low temperature data set refined to a generate a more accurate structure than previously reported. In both structures, the bond lengths and angles are as would be expected for square-planar platinum(II) complexes. In both instances, the platinum complex sits on an inversion center in the crystal lattice and

necessarily assumes the anti conformation (Figure 7). The interatomic distances and angles of the newly reported structure of **6** are also as expected, but in this structure the complex has crystallized in both the syn and anti conformers. In all three complexes, including both conformations of **6**, the amine groups ligated to the platinum centers are at equatorial positions on the cyclohexane rings. This conformation is expected, given the lesser degree of steric hindrance experienced by substituents at these positions. As opposed to rotation about the Pt N bond, which the dynamic NMR experiments reported here have indicated is a rather facile and rapid process, flipping of the cyclohexane ring is expected to be unfavorable with such a bulky substituent. The NMR spectra indicate that the axial and equatorial protons do not exchange, even upon heating to 60 °C.

### 3.7. Characterization of 1, 3, and 5

The tetraammineplatinum(II) halide salts **1**, **3**, and **5** are all readily prepared by reaction of the corresponding tetrahaloplatinates (prepared in situ) with cyclohexylamine. Only the iodo salt **5** could be spectroscopically studied because it could be dissolved without chemical modification. The chloro and bromo complexes require heating to dissolve in DMF, a process that invariably results in partial decomposition to form species in which coordinated cyclohexylamine ligands are replaced by halide ions. These species are evidenced by coloration of the solution and are detected by ESI-MS. In the gas phase, the complex cation appears to degrade readily, even under the relatively gentle ESI conditions, as indicated by the appearance of $[NH_3C_6H_{11}]^+$, $[M\text{-}(NH_2C_6H_{11})_2\text{-}H]^+$, and $[M\text{-}(NH_2C_6H_{11})+X]^+$ signals in ESI-MS measurements of **1**, **3**, and **5.** The conversion from **1**, **3**, and **5** to **2**, **4**, and **6**, respectively, may be facilitated by the bulkiness of the ligands, which serves to destabilize the tetraammineplatinum(II) cation.

The crystal structures of **1**, **3**, and **5** show the cation to have bond distances and angles as expected for a Pt(II) complex. An interesting aspect of all of these structures is that, as we proceed about the platinum center, the rings of the cyclohexylamine ligands are oriented up-up-down-down as opposed to the less sterically encumbering up-down-up-down conformation (Figure 8). There appears to be no significant drive to favor one conformation over the other apart from steric repulsion, and so this particular arrangement of the ligands is most likely induced by crystal packing forces. The lattice is held together by hydrogen bonds between the amine hydrogen atoms and the halide counterions as well as close contacts between the cyclohexyl rings.

## 4. Conclusion

A century has passed since Alfred Werner was awarded the Nobel Prize for his foundation of coordination theory and the field may in some ways be considered a mature branch of inorganic chemistry. The powerful notions of structure and symmetry embodied in coordination chemistry, however, continue to capture the attention and imagination of experienced and neophyte inorganic chemists alike, and work in this field is still vibrant today. Here we have reported an investigation into the dynamic conformational isomerization of *trans*-$[Pt(NH_2C_6H_{11})_2I_2]$, spurred by a chance crystallographic finding. The inability to spectroscopically observe the two distinct isomers under the conditions employed has been rationalized through the use of physical models and computational chemistry. These computational models were also used to evaluate the validity of the thermodynamic parameters of the isomerization that were extracted from the VT NMR data.

While exploring this isomerism, the thermal instability of $[Pt(NH_2C_6H_{11})_4]X_2$ (X= Cl, Br, I) was observed and exploited in the preparation of the corresponding series *trans*-$[Pt(NH_2C_6H_{11})_2X_2]$. This chemistry was found to parallel some of the earliest reactions used to prepare compounds to support the development of Werner's coordination theory.

## Supplementary Material

Refer to Web version on PubMed Central for supplementary material.

## Acknowledgments

This work was supported by grant CA034992 from the National Cancer Institute. Spectroscopic instrumentation at the MIT DCIF is maintained with funding from NIH Grant 1S10RR13886-01. T.C.J. has received partial funding from the Harvard/MIT CCNE, NIH grant 5-U54-CA151884. Justin J. Wilson is gratefully acknowledged for helpful discussions and for assistance with the preparation of the manuscript.

## References

1. Kauffman, GB. Alfred Werner founder of coordination chemistry. Springer-Verlag; Berlin, New York: 1966.
2. Nobelstiftelsen, Chemistry. Published for the Nobel Foundation by Elsevier Pub. Co; Amsterdam, New York: 1964.
3. Hantzsch A, Werner A. Ber. 1890; 23:11–30.
4. Kauffman GB. J Chem Educ. 1966; 43:155–165.
5. Kauffman, GB. Part 1: The Selected Papers of Alfred Werner. Dover Publications; New York: 1968. Classics in Coordination Chemistry.
6. Esteban S. J Chem Educ. 2008; 85:1201–1203.
7. Berzelius JJ. Ann Chim Phys. 1831; 46:113–147.
8. Moss GP. Pure Appl Chem. 1996; 68:2193–2222.
9. Kauffman GB. Coord Chem Rev. 1973; 11:161–188.
10. Pitzer KS. J Chem Phys. 1937; 5:469–472.
11. MacDermott TE, Barfoed S. Acta Chem Scand. 1970; 24:924–930.
12. Jensen KG, Soling H, Thorup N. Acta Chem Scand. 1970; 24:908–918.
13. Werner A, Grün A. Ber. 1905; 38:4033–4040.
14. Jørgensen SM. Z Anorg Chem. 1899; 19:78–80.
15. Kelland LR, Abel G, McKeage MJ, Jones M, Goddard PM, Valenti M, Murrer BA, Harrap KR. Cancer Res. 1993; 53:2581–2586. [PubMed: 8388318]
16. APEX2, APEX2, 2008-4.0. Bruker AXS, Inc; Madison, WI: 2008.
17. SAINT, SAINT: SAX Area-Detector Integration Program, 2008/1. University of Göttingen; Göttingen, Germany: 2008.
18. Sheldrick, GM. SADABS: Area-Detector Absorption Correction. University of Gottingen; Gottingen, Germany: 2008.
19. XPREP, XPREP, 2008/2. Bruker AXS; Madison, WI: 2008.
20. Sheldrick, GM. SHELXTL-97. University of Göttingen; Göttingen, Germany: 2000.
21. Sheldrick GM. Acta Crystallogr A. 2008; 64:112–122. [PubMed: 18156677]
22. Müller P. Crystallogr Rev. 2009; 15:57–83.
23. Spek, AL. PLATON, A Multipurpose Crystallographic Tool. Utrecht University; Utrecht, The Netherlands: 2008.
24. Zanotti G, Delpra A, Bombieri G, Tamburro AM. Acta Crystallogr B. 1978; 34:2138–2141.
25. Lock CJL, Zvagulis M. Acta Crystallogr B. 1980; 36:2140–2142.
26. Rochon FD, Kong PC. Can J Chem. 1986; 64:1894–1896.
27. Siegel JS, Anet FAL. J Org Chem. 1988; 53:2629–2630.
28. Corey RB, Pauling L. Rev Sci Instrum. 1953; 24:621–627.
29. Koltun WL. Biopolymers. 1965; 3:665–670. [PubMed: 4158989]
30. Frisch, MJ.; Trucks, GW.; Schlegel, HB.; Scuseria, GE.; Robb, MA.; Cheeseman, JR.; Montgomery, J.; JA; Vreven, T.; Kudin, KN.; Burant, JC.; Millam, JM.; Iyengar, SS.; Tomasi, J.; Barone, V.; Mennucci, B.; Cossi, M.; Scalmani, G.; Rega, N.; Petersson, GA.; Nakatsuji, H.;

Hada, M.; Ehara, M.; Toyota, K.; Fukuda, R.; Hasegawa, J.; Ishida, M.; Nakajima, T.; Honda, Y.; Kitao, O.; Nakai, H.; Klene, M.; Li, X.; Knox, JE.; Hratchian, HP.; Cross, JB.; Adamo, C.; Jaramillo, J.; Gomperts, R.; Stratmann, RE.; Yazyev, O.; Austin, AJ.; Cammi, R.; Pomelli, C.; Ochterski, JW.; Ayala, PY.; Morokuma, K.; Voth, GA.; Salvador, P.; Dannenberg, JJ.; Zakrzewski, VG.; Dapprich, S.; Daniels, AD.; Strain, MC.; Farkas, O.; Malick, DK.; Rabuck, AD.; Raghavachari, K.; Foresman, JB.; Ortiz, JV.; Cui, Q.; Baboul, AG.; Clifford, S.; Cioslowski, J.; Stefanov, BB.; Liu, G.; Liashenko, A.; Piskorz, P.; Komaromi, I.; Martin, RL.; Fox, DJ.; Keith, T.; Al-Laham, MA.; Peng, CY.; Nanayakkara, A.; Challacombe, M.; Gill, PMW.; Johnson, B.; Chen, W.; Wong, MW.; Gonzalez, C.; Pople, JA. Gaussian 03, Revision B.02. Gaussian, Inc; Pittsburgh PA: 2003.

31. Rappe AK, Casewit CJ, Colwell KS, Goddard WA, Skiff WM. J Am Chem Soc. 1992; 114:10024–10035.
32. Adamo C, Barone V. J Chem Phys. 1999; 110:6158–6170.
33. Hay PJ, Wadt WR. J Chem Phys. 1985; 82:270–283.
34. Hay PJ, Wadt WR. J Chem Phys. 1985; 82:299–310.
35. Peng CY, Schlegel HB. Isr J Chem. 1993; 33:449–454.
36. Peng CY, Ayala PY, Schlegel HB, Frisch MJ. J Comput Chem. 1996; 17:49–56.
37. Khokhar AR, Deng YJ, Albaker S, Yoshida M, Siddik ZH. J Inorg Biochem. 1993; 51:677–687. [PubMed: 8409984]
38. Werner A. Z Anorg Chem. 1893; 3:267–330.
39. Jørgensen SM. J Prakt Chem. 1886; 33:489–538.
40. Peyrone M. Liebigs Ann. 1844; 51:1–29.
41. Chernyaev II. Ann Inst Platine (USSR). 1926; 4:243–275.
42. Kauffman GB. J Chem Educ. 1977; 54:86–89.
43. Rochon FD, Buculei V. Inorg Chim Acta. 2005; 358:2040–2056.
44. Hoffmann, R. Personal communication to E. G. Lewars in 2009; Recorded in Computational chemistry, Chapter 5: Ab initio calculations. p. 365
45. Westheimer FH, Mayer JE. J Chem Phys. 1946; 14:733–738.
46. Hill TL. J Chem Phys. 1946; 14:465–465.
47. McClurg RB, Flagan RC, Goddard WA. J Chem Phys. 1997; 106:6675–6680.
48. Truhlar DG. J Comput Chem. 1991; 12:266–270.
49. Ayala PY, Schlegel HB. 1998; 108:2314–2325.
50. Jackman, LM.; Cotton, FA.; Adams, RD. Dynamic nuclear magnetic resonance spectroscopy. Academic Press; New York: 1975.
51. Souchard JP, Wimmer FL, Ha TTB, Johnson NP. J Chem Soc Dalton. 1990:307–310.
52. Pearson RG. J Am Chem Soc. 1963; 85:3533–3539.
53. Ahrland S, Chatt J, Davies NR. Q Rev Chem Soc. 1958; 12:265–276.
54. Bernstein, J. Polymorphism in Molecular Crystals. Clarendon Press; Oxford: 2002.

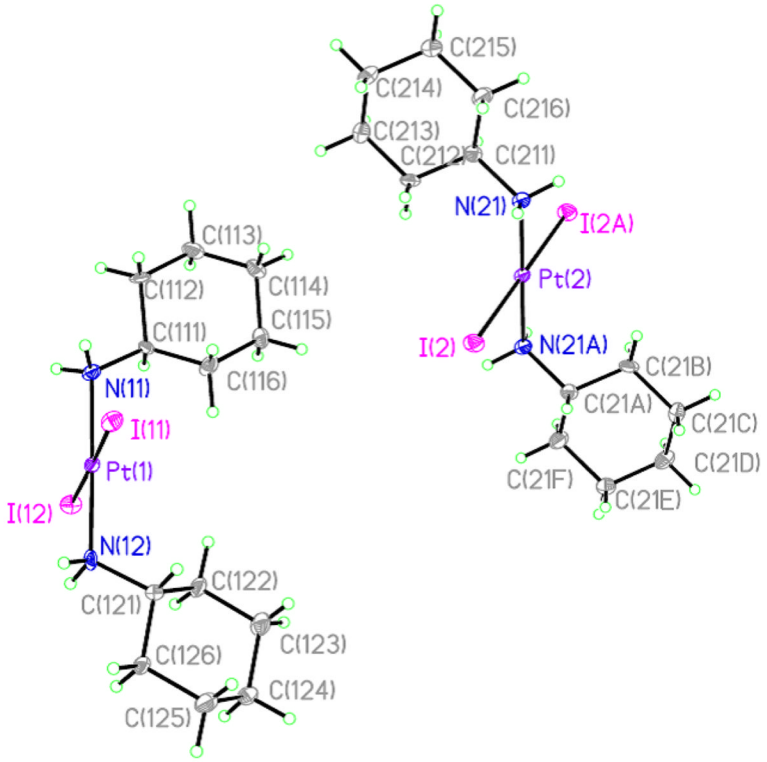


**Figure 1.**
The syn and anti conformers of **6** as present in the crystal structure. Ellipsoids are drawn at the 50% probability level.

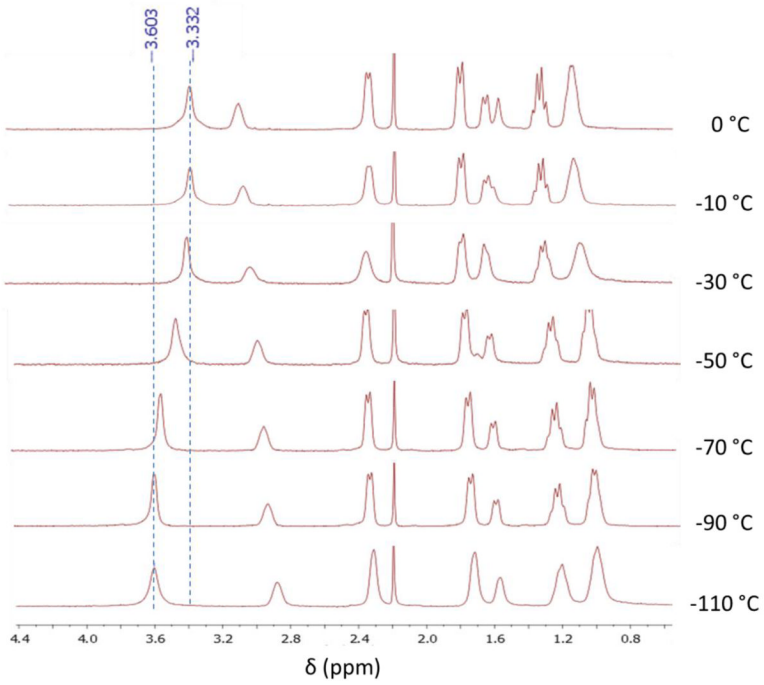


**Figure 2.**

VT NMR of **6** in DCFM-*d*. The shift in the amine peak is highlighted with dashed lines. The signal between 2.9 and 3.1 ppm arises from the CH group directly attached to the amine nitrogen. All other signals arise from cyclohexyl ring protons or solvent as indicated in the Supplementary data (Fig S1).

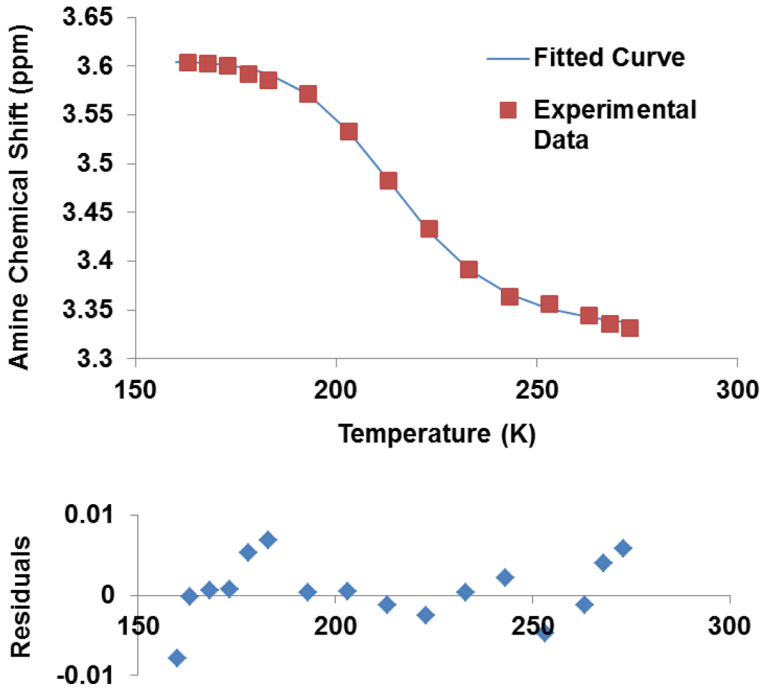


**Figure 3.**

Plot of amine chemical shift against temperature. The theoretical curve was fit according to eq 2 with $\delta_{anti}$ = 3.605 ppm, $\delta_{syn}$ = 3.330 ppm, ΔH° = 30.127 kJ mol$^{-1}$, and ΔS° = 139.6 J mol$^{-1}$ K$^{-1}$.

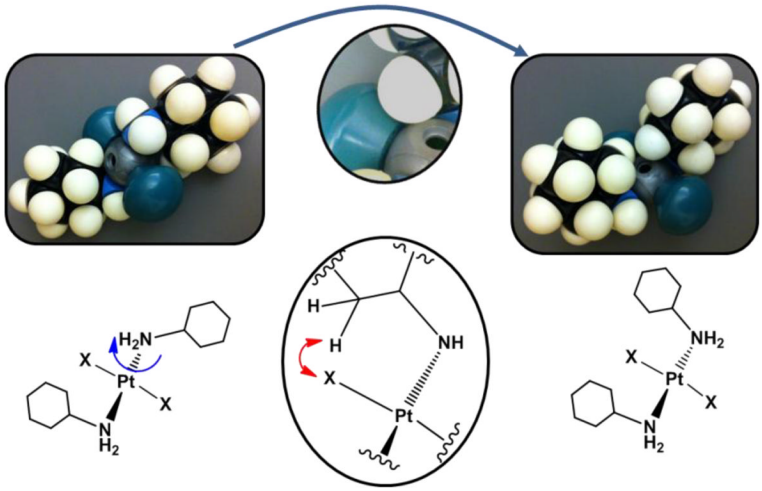


**Figure 4.**
CPK models of the anti (left) and syn (right) conformers of **2** with corresponding line diagrams below. Manual rotation from one conformer to the other causes a clash between a ring hydrogen atom and the halide ligand, as shown in the middle.

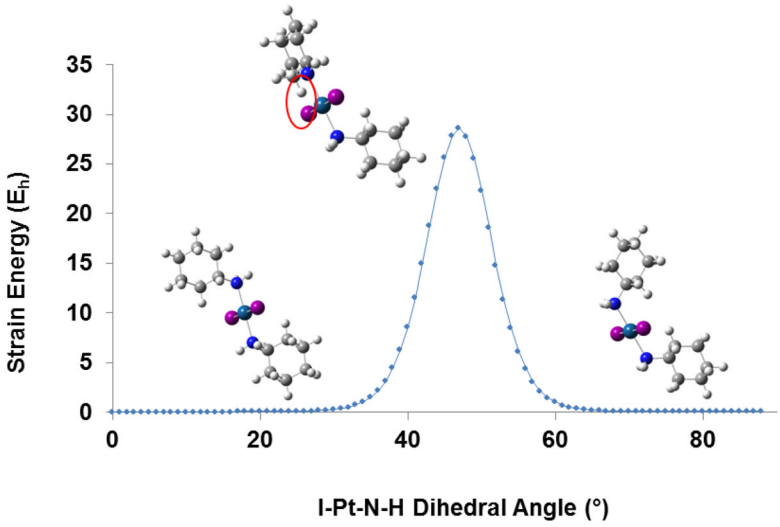


**Figure 5.**
MM rigid surface scan about the Pt–N bond. Structures are shown of the anti (left) and syn (right) conformers as well as the maximum along the PES (middle). The red circle highlights the steric interaction between the H and I atoms.

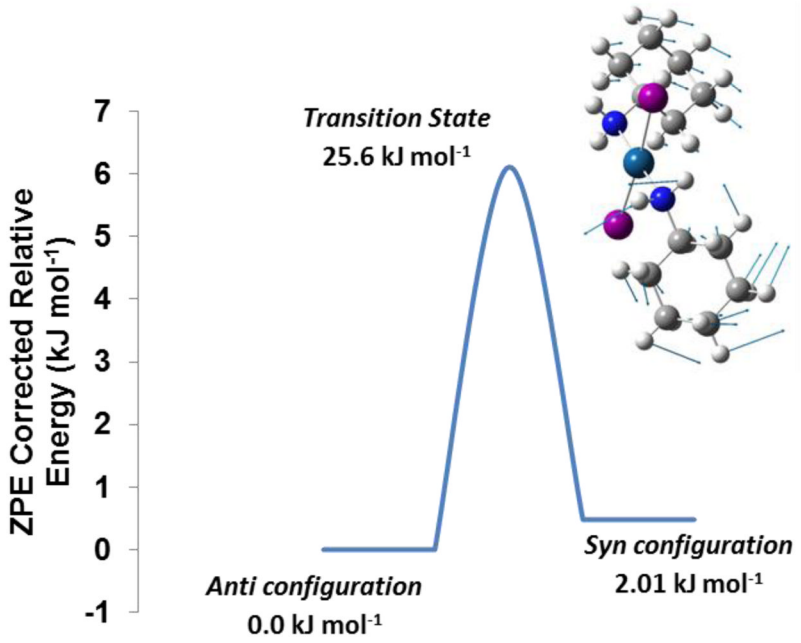


**Figure 6.**
Energy level diagram from gas phase DFT calculations. The molecular diagram depicts the calculated transition state and the vectors represent the single vibrational mode (rotation about the Pt–N bond) calculated to have an imaginary frequency.

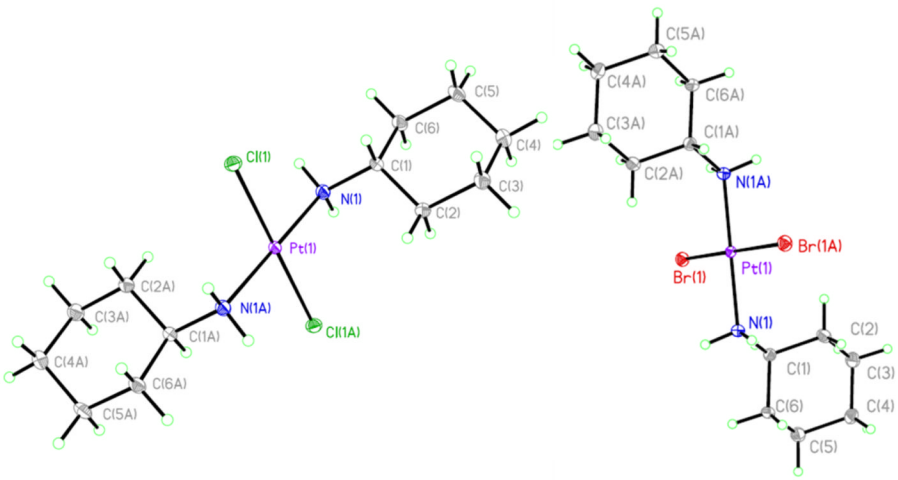


**Figure 7.**
Molecular diagrams of **2** (left) and **4** (right). Ellipsoids are drawn at the 50% probability level.

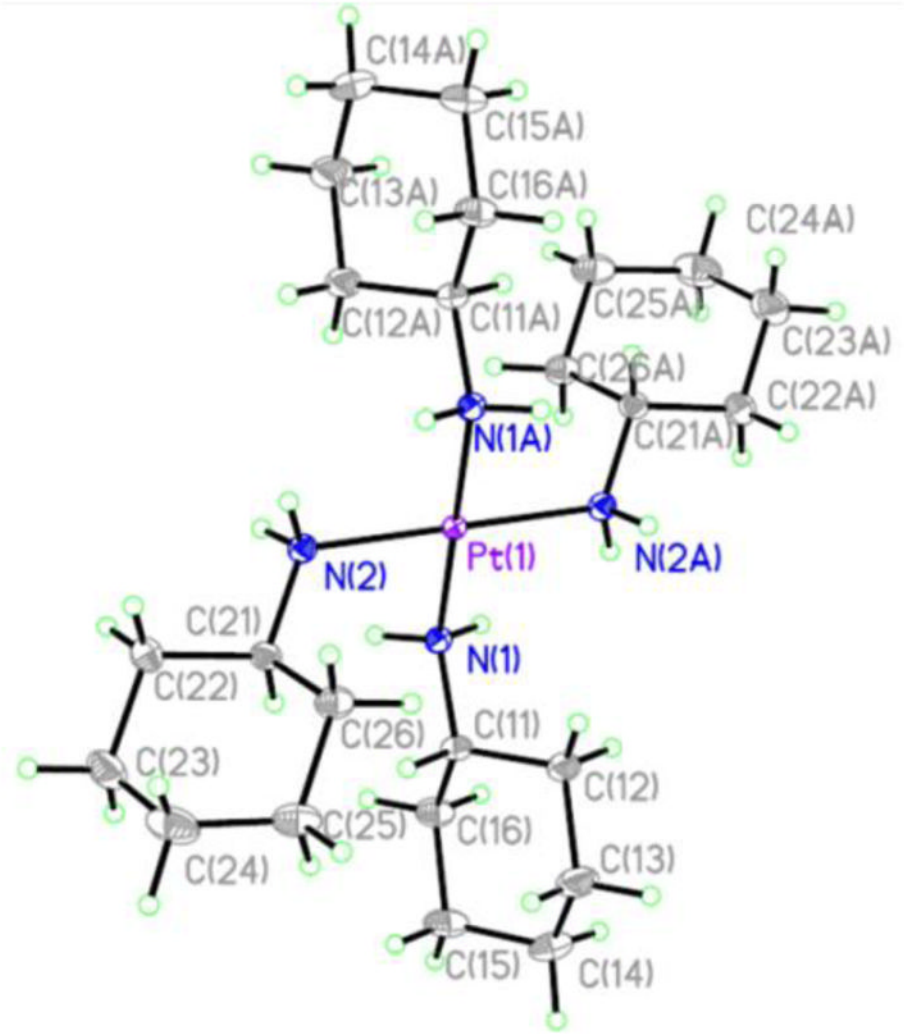


**Figure 8.**
Thermal ellipsoid plot of the complex cation of **1**. Ellipsoids are drawn at the 50% probability level.

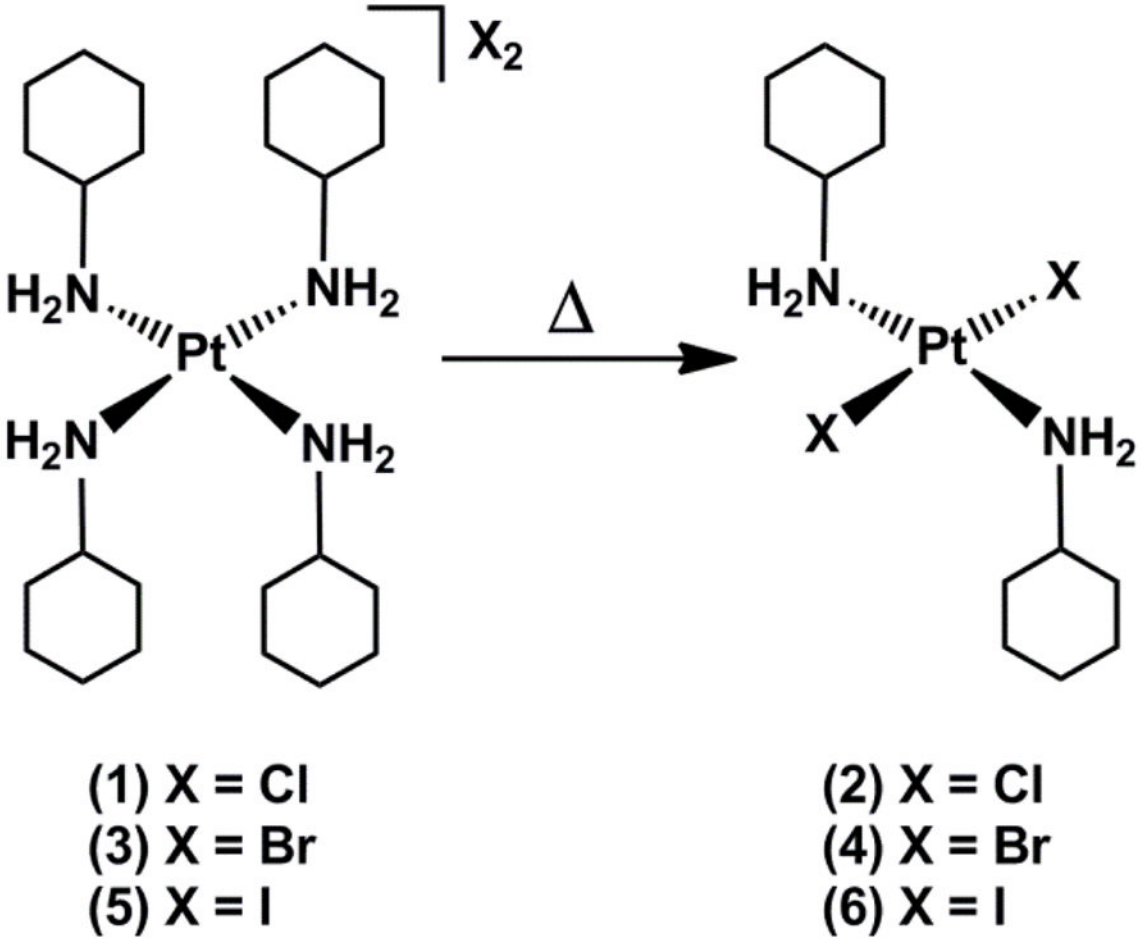


**Scheme 1.**
The compounds and reaction investigated in this study. Compound **6** can also be prepared as indicated in Scheme 2.

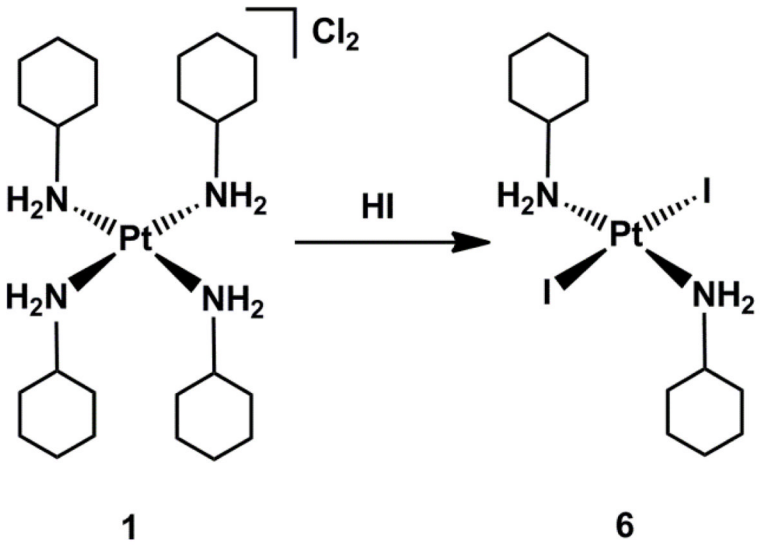


**Scheme 2.**
Preparation of **6** according to Jørgensen's rule.

**Table 1**

Crystallographic parameters for **1**, **2**•2DMF, **3**, **4**, **5**, and **6.**

| | **1** | **2•2DMF** | **3** | **4** | **5** | **6** |
|---|---|---|---|---|---|---|
| Formula | $C_{24}H_{52}Cl_2N_4Pt$ | $C_{18}H_{40}Cl_2N_4O_2Pt$ | $C_{24}H_{52}Br_2N_4Pt$ | $C_{12}H_{26}Br_2N_2Pt$ | $C_{24}H_{52}I_2N_4Pt$ | $C_{12}H_{26}I_2N_2Pt$ |
| Formula weight | 662.68 | 610.52 | 751.61 | 553.26 | 845.59 | 647.24 |
| Space group | $P2_1/c$ | $P\bar{1}$ | $P\bar{1}$ | $P2_1/c$ | $P\bar{1}$ | $P\bar{1}$ |
| *a,* Å | 12.7318(17) | 6.1518(6) | 6.3395(7) | 6.1614(5) | 6.7701(5) | 9.4215(8) |
| *b,* Å | 10.7966(14) | 8.0596(8) | 10.3789(12) | 8.6696(7) | 10.4276(7) | 11.2597(10) |
| *c,* Å | 11.6467(16) | 12.6037(12) | 12.3584(14) | 15.2029(12) | 12.2655(8) | 12.6232(11) |
| α, ° | | 76.2260(10) | 110.489(2) | | 110.2170(10) | 105.3630(10) |
| β, ° | 111.360(2) | 76.2260(10) | 102.599(2) | 96.8440(10) | 101.5970(10) | 92.6850(10) |
| γ, ° | | 89.3090(10) | 97.082(2) | | 98.6220(10) | 98.4830(10) |
| *V,* Å$^3$ | 1491.0(3) | 588.11(10) | 725.42(14) | 806.30(11) | 772.96(9) | 1271.94(19) |
| *Z* | 2 | 1 | 1 | 2 | 1 | 3 |
| *T,* K | 100(2) | 100(2) | 100(2) | 100(2) | 100(2) | 100(2) |
| $\mu$(Mo Kα), mm$^{-1}$ | 4.897 | 6.196 | 7.608 | 13.641 | 6.552 | 11.900 |
| θ range, ° | 1.72 to 28.76 | 1.72 to 28.80 | 1.83 to 27.04 | 2.70 to 28.39 | 1.84 to 28.33 | 1.68 to 27.92 |
| total no. of data | 29730 | 10483 | 13197 | 15547 | 15245 | 24450 |
| no. of unique data | 3869 | 3037 | 3173 | 2025 | 3806 | 6046 |
| no. of parameters | 142 | 126 | 142 | 79 | 142 | 232 |
| completeness to θ (%) | 99.7 | 99.1 | 99.7 | 99.9 | 99.2 | 99.2 |
| $R_1$[a] (%) | 1.17 | 1.27 | 1.92 | 1.44 | 1.40 | 2.53 |
| $wR_2$[b] (%) | 2.75 | 3.05 | 4.60 | 3.47 | 3.31 | 4.45 |
| GOF[c] | 1.055 | 1.033 | 1.029 | 1.110 | 1.049 | 0.994 |
| max, min peaks, e Å$^{-3}$ | 0.85 and −0.68 | 1.01 and −0.73 | 1.97 and −0.82 | 1.01 and −1.25 | 1.09 and −0.71 | 1.29 and −0.80 |

[a] $R_1=\Sigma||F_o|-|F_c||/\Sigma|F_o|$.

[b] $wR_2=\{\Sigma[w(F_o^2-F_c^2)^2]/\Sigma[w(F_o^2)^2]\}^{1/2}$.

[c] $GOF=\{\Sigma[w(F_o^2-F_c^2)^2]/(n-p)\}^{1/2}$, where $n$ is the number of data and $p$ is the number of refined parameters.